Structural characterization of toxic oligomers that are kinetically trapped during α-synuclein fibril formation

Serene W. Chen, Srdja Drakulic, Emma Deas, Myriam M. Ouberai, Francesco A. Aprile, Rocío Arranz, Samuel Ness, Cintia Roodveldt, Tim Guilliams, Erwin De Genst, David Klenerman, Nicholas W. Wood, Tuomas P.J. Knowles, Carlos Alfonso, Germán Rivas, Andrey Y. Abramov, José María Valpuesta, Christopher M. Dobson and Nunilo Cremades

Correspondence should be addressed to N.C (nc347@cam.ac.uk) or C.M.D. (cmd44@cam.ac.uk)

Supplemental Information

Supplemental Experimental Procedures

Preparation of purified αS oligomeric samples

αS oligomeric samples were prepared on the basis of previous protocols (1-10). Monomeric fractions of αS solutions, in which size-exclusion chromatography had been utilized in the last step of the purification process of the protein, were dialysed into water. Six mg (ca. 1.5 – 3 mL) of the dialysed protein were placed in 15mL falcon tubes, flash frozen in liquid nitrogen, and then lyophilized for ca. 48h at room temperature using either an EC MicroModulyo freeze dryer unit (EC Apparatus Inc., USA) attached to an Edwards XDS-10 vacuum pump (Edwards Limited, UK), or a Heto Lyolab 3000 freeze dryer unit (Heto-Holten A/S, Denmark) attached to an Edwards nXDS-10i vacuum pump (Edwards Limited, UK). The lyophilized protein was then stored at -20 ^{o}C

prior to use. In order to prepare enriched oligomeric samples, the lyophilized protein was subsequently resuspended in PBS buffer, pH 7.4, to give a final concentration of ca. 800 μM (12 mg/ml), and passed through a 0.22 μm cut off filter immediately prior to incubation at 37 °C for 20-24 h without agitation or the application of any other process that could induce shear and hence accelerate the conversion of monomers and oligomers into fibrils (11, 12). During this time, a very small number of fibrillar species were observed to form and removed by ultracentrifugation for 1 h at 90,000 rpm (using a TLA-120.2 Beckman rotor; 288,000 x *g*). Only a very few fibrillar-like species of very small size still remained in the supernatant, as revealed in AFM and negatively stained TEM images, and they were insignificant in quantity compared to the oligomeric species present in the final preparation (estimated to be < 0.3% in number of species and < 3% in protein mass according to the analysis of TEM images). The excess of monomeric protein, as well as the low levels of very small oligomers, were removed by means of multiple filtration steps (using 100 kDa cut-off membranes) in order to enrich the sample in pure oligomeric species of αS. The concentrations of the final solutions of oligomers were estimated from the absorbance at 275 nm using a molar extinction coefficient of 5600 $M^{-1}.cm^{-1}$ (no significant changes in the molar extinction coefficient value were found for the oligomeric species relative to the monomeric protein). The concentration values given in the manuscript represent the total mass concentration of protein, i.e. the total concentration in monomer equivalents.

Preparation of αS fibrils

Human αS was over-expressed and purified as a monomeric fraction from *E.coli* as described previously (13). Fibrils were prepared by incubating monomeric αS at 70 μM (1 mg/ml) in PBS buffer pH 7.4 (0.1 M ionic strength; 0.01% NaN_3 was added to prevent bacterial growth during aggregation) at 37 °C, under constant agitation (200 rpm) for 4-6 days. After this time, each sample was centrifuged (15 min at 13200 rpm) and the fibrillar pellet washed twice with PBS before being

resuspended into the appropriate volume of PBS. The final concentration of fibrils, that was typically ca. 100 μM in each sample, was estimated by measuring the absorbance at 275 nm using a molar extinction coefficient of 5600 $M^{-1}.cm^{-1}$ after disaggregating an aliquot by the addition of guanidinium chloride to a final concentration of 4 M; this concentration therefore represents the total monomeric concentration present in the fibrillar sample.

Possible chemical modifications or other changes in the protein molecules during the generation of the different assembled species were ruled out by mass spectrometric analysis (where identical results were obtained for the monomeric, oligomeric and fibrillar αS samples).

Preparation of fluorescently labeled αS oligomers for smFRET studies

For the preparation of fluorescently labeled oligomers, the procedure was the same as that described for the unlabeled oligomers at the main text but mixing 400 μM of Alexa Fluor-488 (AF488) labeled protein and 400 μM Alexa Fluor-647 (AF647) labeled protein, bringing the total protein concentration to 800 μM in PBS. In order to label the protein, the A90C mutant variant of αS was expressed in, and purified from, *E.coli* as described previously (13), and then treated with either maleimide-modified AF488 or AF647 dyes (Invitrogen), via the cysteine thiol moiety (at labeling efficiencies of 98 ± 3 % for both cases as estimated by mass spectrometry). The labelled protein was separated from the excess of free dye by a P10 desalting column with Sephadex G25 matrix (GE Healthcare), divided into aliquots, flash frozen and lyophilised; the lyophilised protein was then stored at -20° C. Concentrations of the labelled proteins were estimated from the absorbance of the fluorophores and correspond to the total monomer equivalent.

In order to generate FRET active oligomers we mixed equal concentrations of monomeric αS protein labeled with either AF488 (FRET donor) or AF647 (FRET acceptor), as described previously (12), and then prepared solutions containing purified doubly labelled oligomers as described above. The possibility that any significant alteration of the oligomer structure could occur

as a result of the presence of the dyes was ruled out by comparing the secondary structure content and the AFM-derived dimensions of the labeled and unlabeled oligomers and finding them to be identical (see Figure S7).

Preliminary characterization of the size distribution of the purified oligomeric samples

- HPLC-SEC: HPLC-SEC analysis was performed by injecting samples of αS oligomers onto an Agilent Bio SEC-3 column (300 Å pore size) using an Agilent Infinity 1260 series HPLC. The elution volume of the oligomers was compared with human plasma immunoglobulin M (1026kDa (14)) (Millipore) and a set of high molecular weight protein standards (Bio-Rad) consisting of thyroglobulin (670kDa), γ-globulin (158kDa), ovalbumin (44kDa), myoglobin (17kDa) and vitamin B12 (1.35kDa). All HPLC runs were performed in pH 7.4 PBS buffer at a flow rate of 0.5 ml/min and monitored by absorbance at 214nm.

- Native electrophoresis: Native electrophoresis analysis was performed on 10 μg of purified monomeric, oligomeric and fibrillar αS samples using NativePAGE™ Bis-Tris 4-16% precast minigel system (Invitrogen), according to manufacturer instruction.

- Dynamic Light Scattering measurements: The intensity weighted mean hydrodynamic diameter with polydispersity index PdI (a parameter used to describe the width of the size distribution) and the diameter intensity distribution profile of monomeric (45 μM), oligomeric (5 μM) and fibrillar (3 μM) αS species in PBS at 25°C were determined by DLS using a Zetasizer Nano ZS (Malvern Instruments) at a back scattering angle of 173°.

Atomic force microscopy

A PicoPlus AFM instrument with a PicoSPM II controller from Molecular Imaging (Agilent) was used for the AFM imaging studies. Images were acquired at room temperature in air using the AC Mode with NSC36/no Al cantilevers (Mikromasch, with force constants varying from 0.6 to 2

N/m). For each imaging experiment, an aliquot of the corresponding αS species was deposited onto freshly cleaved mica and incubated for 10 min, followed by washing with deionised water and drying under a stream of nitrogen.

Bulk spectroscopic measurements

- Far-UV CD: Far-UV CD spectra of the different αS species were acquired in PBS at 20 °C. The proteins solutions were diluted to a final concentration of ca. 10 µM and spectra were acquired using a 1 mm path length cuvette and a J-810 Jasco spectropolarimeter (Tokyo, Japan), equipped with a thermostated cell holder.

- FT-IR: FT-IR spectra of monomeric, oligomeric and fibrillar αS solutions of ca. 100 µM (the oligomeric samples were at concentrations of ca. 400 µM) in PBS were recorded and analysed in a Bruker BioATRCell II using a Bruker Equinox 55 FT-IR spectrophotometer (Bruker Optics Limited, UK) equipped with a liquid nitrogen cooled mercury cadmium telluride (MCT) detector and a silicon internal reflection element (IRE). For each spectrum, 256 interferograms were co-added at 2 cm^{-1} resolution, and the buffer background was independently measured and subtracted from each protein spectrum before curve fitting of the amide I region (1720-1580 cm^{-1}). Data processing, consisting of atmospheric compensation, baseline subtraction, second derivative analysis, and deconvolution with Gaussian/Lorentzian curves using a Levenberg-Marquardt algorithm was performed with the Opus software package (Bruker Optics Limited, UK). Data presented are a result of the fitting of 3 independent FTIR spectra for each protein sample. For comparison all absorbance spectra were normalized.

In order to estimate the relative fraction of β-sheet content in each protein sample, the deconvolution analysis with Gaussian/Lorentzian curves for each spectra recorded was performed. The calculation of the second derivatives was used to identify peak maxima. For the spectra of the oligomeric samples six Gaussian distributions were needed to fit the data, while only five were used

for the spectra of the fibrillar samples (see Figure S3). The different Gaussian distributions were then assigned to contributions from either β-sheet secondary structure or random coil according to the position of their peaks (15) (see Figure S3; note that the values of relative content of secondary structure content of a protein sample obtained in this way represent only estimates).

The analysis of the FT-IR spectra allows the distinction between parallel and anti-parallel β-sheet structures based on the analysis of the amide I (1700-1600 cm^{-1}) region (16). In anti-parallel β-sheet structures, the amide I region displays two typical components: the major one has an average wavenumber located at ca. 1630-1620 cm^{-1}, whereas the minor component, approx. 5-fold weaker than the major one, is characterized by an average wavenumber at 1695 cm^{-1}. For parallel β-sheet structures, the amide I region displays only the major component around 1630-1620 cm^{-1}.

The similar positions of the peaks of the Gaussian distributions in the oligomers and the fibrils reflect a high similarity in the type of secondary structure organization present in both forms of the protein, suggesting that they differ mainly in the extent of β-sheet versus disordered content as well as the overall β-sheet arrangement (mainly parallel for the fibrillar state and anti-parallel for the oligomeric state).

- Fluorescence: Fluorescence measurements were carried out on a Varian (Palo Alto, CA, USA) model Cary Eclipse spectrofluorimeter in a temperature-controlled cell holder, utilising a 2 mm x 10 mm path length cuvette. ThT binding was monitored by exciting the sample at 446 nm and recording the emission fluorescence spectrum from 460 to 600 nm. 10 μM of each protein sample was incubated with 50 μM ThT in PBS for 30 min before fluorescence recording. 8-anilo-1-naphtalene-sulfonic acid (ANS) binding was monitored by exciting the sample at 350 nm and recording the emission from 400 to 650 nm. In this case, 5 μM of each protein sample was incubated with 250 μM ANS in PBS for 30 min before recording the spectra. The extinction coefficient at 350 nm of ANS was taken to be 5000 cm^{-1}M^{-1} (17). For the analysis of ANS binding

to the different protein samples in the presence of urea, the samples were initially incubated for at least 2 hours with urea before the addition of ANS.

Correlation between structural properties and size in the oligomers

As it is challenging to perform FT-IR analysis of protein samples containing urea due to the strong urea absorbance in the region of interest, far-UV CD analysis was used to assess the secondary structure content of protein samples containing urea. The average percentage of β-sheet of the oligomers was estimated by comparing the far-UV CD signals at 220 nm of the oligomers and the monomeric protein at the different urea concentrations (0-1.5 M; see Figure S5 for a detailed analysis of the effect of urea on the structure of the oligomers) with data recorded in the absence of urea, where the β-sheet content was estimated by FT-IR analysis. The estimated β-sheet content for each sample was correlated with the average sedimentation coefficient obtained by AU for the same samples.

A similar analysis was also performed to estimate the relative hydrophobic surface area exposed to the solvent in the oligomers as a function of their size. The extent of hydrophobic surface exposed to the solvent was assessed by comparing the wavelength at the maximum fluorescence emission of ANS of the oligomers at the different conditions as a function of their average sedimentation coefficient obtained by AU and with that found for the monomeric and the fibrillar forms of the protein.

In both cases, we found a good linear correlation:

% β-sheet = 11 ± 6.2 + (1.86 ± 0.45)•S ; R = 0.812, s.d. = 1.54, N = 11

λ_{max} (ANS) = 517 ± 3 − (1.71 ± 0.21)•S ; R = 0.97, s.d. = 0.56, N = 6

where S stands for the averaged sedimentation coefficient of the oligomers, R represents the correlation coefficient, and N is the number of data points used for the correlation.

Electron microscopy and image processing

- Image recording: For transmission-electron microscopy (TEM), aliquots of the purified αS oligomers were applied to previously glow-discharged carbon-coated copper/rhodium grids and stained with 2% uranyl acetate. The negatively-stained samples were observed, and micrographs were taken under minimal-dose conditions, on Kodak SO-163 film in a JEOL JEM1200EXII microscope operated at 100 kV and 60,000 X magnification. Micrographs were digitized using a ZEISS scanner with the step size of 14μm, resulting in a pixel size of 2.33 Å. For cryoelectron microscopy (cryo-EM) experiments, protein aliquots were applied to glow-discharged, holey carbon grids (carbon-coated Quantifoil R 1.2/ R1.3 300 mesh grids) containing an additional continuous thin layer of carbon and plunged into liquid ethane. Images were acquired under minimal dose conditions with a Tecnai F20 transmission electron microscope at 200 kV. The images were taken at a magnification of ~50 000 using a 16 megapixel (Mpx) FEI Eagle CCD camera with a step size of 15 μm; thus the original pixel size of the acquired images was 2.74 Å.

- Image processing: For the TEM images, the contrast transfer function of the each acquired image was estimated using the CTFFIND3 program (18) and corrected at the micrograph level. In both, TEM and cryo-EM images, individual particles were selected manually and extracted using XMIPP software (19). The analysis in both cases was performed using the same procedures. Particle classification was carried out using maximum-likelihood and clustering multi-reference refinement approaches (20, 21), implemented in XMIPP software package, which rendered a large number of class averages (see Figure S6c). The class averages generated in this way, and their corresponding assigned particles, were first visually separated into two main size groups, on the basis of their general dimensions, followed by an iterative procedure consisting of several rounds of 2D classification in order to enable a clearer separation of the two populations (Figure S6d). Homogeneous populations were obtained and averaged for final two-dimensional characterization. For the 3D reconstruction of the two populations that were resolved, several starting reference

models (a "blob" and one based on a "common lines" approach) and initial 3D reconstruction steps based on iterative angular refinement were performed using the EMAN software package (22). All the present refinement program packages exhibit, to some extent, the dependence on the initial reference ("model bias"). This can be overcome by running several independent reconstructions starting from various initial models. There are different methodologies implemented in EMAN that can be employed to generate initial reference maps: "Common lines", in which an initial model is generated using the class averages created in the previous step. This methodology is based on the central section theorem (23), that postulate that Fourier transformation of 2D images, representing the projections of the observed object, constitute the planes of that object in 3D Fourier space. The "Blob" approach generates a geometric object whose dimensions should correspond to the averaged class images. The different strategies converged to a similar solution for the two populations, and one of the models for each population was selected to complete the refinement using a projection matching procedure. The resolution of the reconstructions was determined by the FSC 0.5 criterion, and was found to be 18 Å and 19 Å for the cryo-EM 3D reconstructions of the 10S and 15S oligomer subgroups, respectively, and 26 Å for the two 3D reconstructions of the negatively-stained 10S and 15S oligomers. Visualization of the density maps and atomic structures was performed using UCSF Chimera (24).

Single-molecule FRET data collection and analysis

For the single-molecule FRET analysis of the fluorescently labelled oligomers, a 2 μl aliquot was diluted 10^5-fold by serial dilution with 0.022μm-filtered Tris 25 mM, pH 7.4, 0.1 M NaCl. This buffer was chosen in order to be able to compare the results directly with previously reported data (12). For the analysis, 500 μl of the diluted samples were placed on glass slides that have been treated by incubation for 1h with BSA at 1mg/mL to prevent αS species from adsorbing to the

surface, as we have previously shown (12); the samples were placed on the slides immediately after removal of the BSA solution.

The instrumentation used for smFRET experiments has been described in detail previously (25) as well as the settings for the experimental procedure and analysis (12) (12). During the measurements, the microscope stage was moved at a constant scanning rate of 200 μm.s^{-1} by two orthogonal DC motors (M-112.IDG, Physik Instrumente) so that the encounter rate does not depend on the size of the species being observed. The photon time traces were analyzed by first setting an optimized threshold value for each channel under our conditions of measurement to remove the background noise: a 20 photon.ms^{-1} bin for the donor channel and a 10 photon.ms^{-1} bin for the acceptor channel. After thresholding the raw data, coincident events (due to oligomers exhibiting FRET) are identified and a list of all the fluorescent bursts from such events recorded during the measurement is obtained. From the number of oligomer and total events recorded per second (r_C and r_T, respectively), we obtain the fraction of dual-labeled molecules within the sample:

$$Q = \frac{1}{2}\frac{r_C}{r_T}$$
Eq.1

The ratio of the burst rate of coincident events to the burst rate of total events in the blue channel (r_T) was divided by two to account for the rate of total events in the red channel that cannot be measured but were assumed to be the same as that of the blue channel. The fraction of oligomers (or dual-labeled molecules) was further corrected for the efficiency of detection of coincidence fluorescence; in our experiments we determined this value to be 25 %, using a sample containing only dual-labeled 40bp-dsDNA (25).

The FRET efficiency for each oligomer was calculated from the following expression:

$$E_{FRET} = \frac{I_A}{\gamma I_{DA} + I_A}$$
Eq.2

where I_A and I_{DA} correspond to the acceptor fluorescence intensity and to the donor fluorescence intensity in the presence of acceptor, respectively, and γ to a correction factor that accounts for different quantum yields and detection efficiencies of the donor and acceptor ($\gamma = 0.26$).

A significant number of oligomer events occupied more than 1 time bin (1 ms). For these cases, the maximum brightness recorded per bin (i.e. the brightness recorded during 1 ms when the oligomer crosses the centre of the confocal volume) was used to calculate the FRET efficiency. Large species, i.e. those corresponding to events occupying more than 5 bins, or calculated to be more than 150 mers, were assumed to be fibrillar species and then were excluded from the analysis; very few such species, however, were found in the isolated oligomeric samples.

Limited digestion of protein species with proteinase K

We measured the sensitivity of αS monomers, oligomers and fibrils to proteinase K degradation. The different protein samples were prepared in Tris 25 mM pH 7.4, 0.1 M NaCl instead of PBS buffer because of the insolubility of Ca^{2+}, which is essential for the protease activity, in phosphate buffer. Briefly, aliquots of ca. 25-40 μM of the different protein species were incubated with increasing concentrations of proteinase K (proteinase K from *Tritirachium album*, Sigma-Aldrich) for 20 min at 37 °C, and the reaction quenched by boiling the samples for 5 min. The monomeric samples were then analysed directly by SDS-PAGE gels. The conditions used for the electrophoresis were constant voltage of 200 V, and the run time was 35 min using MES SDS running buffer (Invitrogen protocol). For the analysis of αS oligomers and fibrils, the samples were incubated with guanidine thyocianate at a 3 M final concentration for 1 hour at room temperature in order to dissolve the aggregated species. Finally, the salt concentration of the samples was reduced to ca. 2 M in order to allow a normal electrophoresis running. The quantification of the level of proteinase K resistance was performed using the band in the Coomassie-stained gel corresponding to full-length monomeric αS. The gel analysis was carried out using NIH Image-J software.

For the analysis of fluorescently labelled oligomers, the same procedure was used, although less protein solution was needed in this case, as the quantification was done using the fluorescence properties of the dyes utilizing a Typhoon Trio scanner (Amersham Bioscience). AF488-labeled protein was excited at 488nm and emission collected at 526nm, while AF647-labeled protein was excited at 633nm and emission collected at 670nm. The image analysis was done with ImageQuant TL v2005 software (Amersham Bioscience).

Primary neuronal culture preparations

Mixed neuronal midbrain cultures were prepared from Sprague-Dawley rat pups 3 days postpartum (UCL breeding colony). Subjects were culled via decapitation and the midbrain was dissected into ice-cold HEPES buffered salt solution (Ca^{2+}, Mg^{2+}-free; Gibco-Invitrogen, Paisley, UK). The tissue was minced and trypsinized (0.25% for 15 min at 37 °C), triturated and plated on poly-D-lysine-coated coverslips and cultured in neurobasal A medium (Gibco-Invitrogen) supplemented with B-27 (Gibco-Invitrogen) and 2 mM L-glutamine. Cultures were maintained at 37 °C in a humidified atmosphere of 5% CO_2 and 95% air, fed once a week and maintained for a minimum of 14 days before experimental use. Neurons were easily distinguishable from glia: they appeared phase bright, had smooth rounded somata and distinct processes, and lay just above the focal plane of the glial layer. Cells were used at 14–16 days *in vitro*. Animal husbandry and experimental procedures were performed in full compliance with the United Kingdom Animal (Scientific Procedures) Act of 1986.

ROS measurements

Fluorescence measurements were obtained on an epifluorescence-inverted microscope equipped with a 20× fluorite objective. ROS production was measured as the rate of increase in the ratio of dihyroethidium (HEt) fluorescence between its oxidized and non-oxidized forms. Measurements

involving excitation at 530 nm and emission collected above 560 nm were used to quantify the oxidized form (ethidium), whereas measurement of excitation at 360 nm and emission collected from 405 to 470 were used for the reduced form (hydroethidium). For measurement of cytosolic ROS production, dihydroethidium (2μM) was present in the solution during the experiment. No preincubation ('loading') was used for dihydroethidium to limit the intracellular accumulation of oxidized products. All data reported in this study were obtained from at least five coverslips and 3–4 different cell and sample preparations. The solutions with the different αS species were added at a final concentration of 40 nM mass concentration.

In vitro membrane permeability assay

Permeabilization of lipid membranes induced by αS species and melittin was monitored by following the leakage of entrapped calcein within LUVs (26). The lipid concentration was adjusted to 5 μM. LUVs (100 nm diameter) were mixed with αS species and melittin and incubated at room temperature for up to 2 hours. All fluorescence determinations were performed on a Varian (Palo Alto, CA, USA) model Cary Eclipse spectrofluorimeter, utilising a 2 mm x 10 mm path length cuvette using λ_{exc} and λ_{em} of 485 nm and 520 nm, respectively. The percentage of calcein released was defined as:

$\%_{release} = [(F\text{-}F_{contr})/(F_{tot}\text{-}F_{contr})]\times100$

where F is the fluorescence signal measured in the presence of αS species and melittin, F_{contr} is the fluorescence signal measured at the same time in the control LUVs, and F_{tot} is the total fluorescence signal obtained after complete disruption of LUVs using Triton X-100 (1% v/v).

Data presented in Figure 5E represent the average values and standard deviations of triplicates. The statistical analysis was performed using one-way ANOVA, correlating the values obtained for the αS oligomers with the values obtained for monomeric and fibrillar αS, and for mellitin, considering each lipid composition as a family. We estimated that there could be up to

10% of deviations of the experimental values when comparing different series of experiments, although the differences in signal obtained for each protein species when compared across all the experimental series were very similar, with an error of ca. 6%.
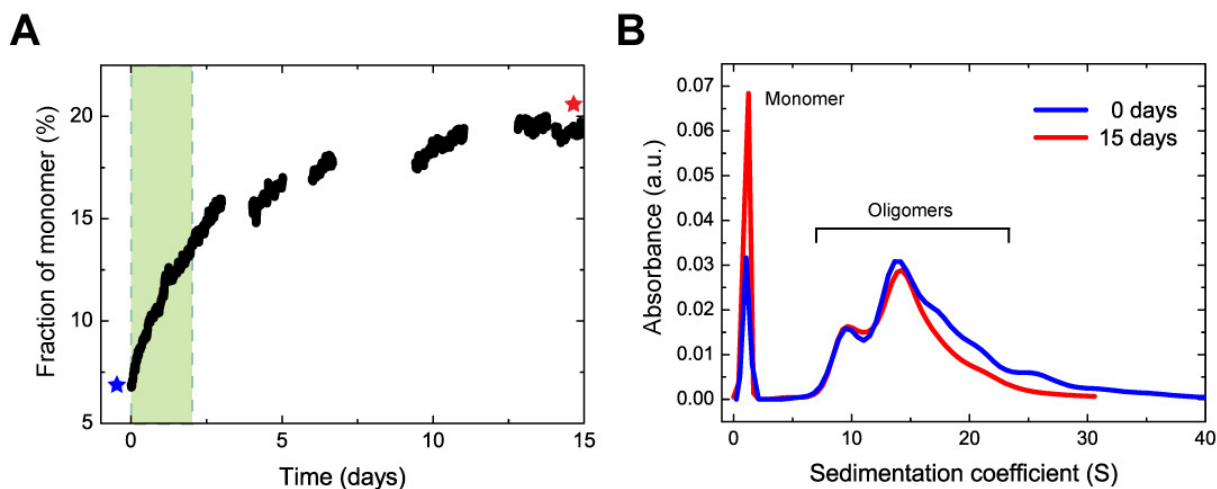
Figure S1. Kinetic stability of the oligomeric sample. The kinetic stability of the oligomeric sample was assessed by far-UV CD in order to monitor the fraction of monomeric protein in the sample as a function of time (A), as well as by AU at different time points in order to confirm the fraction of monomer in the sample obtained by far-UC CD, to evaluate the size distribution of the oligomeric species and to rule out the formation of larger aggregated species (B). The sedimentation coefficient profiles at 0 and 15 days after preparing the oligomeric sample are very similar; The profile at 15 days shows a slight decrease in the fraction of oligomers in the sample (corresponding to the reduction in number of the largest oligomeric species), concomitant with a slight increase in the fraction of monomeric protein (from ca. 7% to ca. 20%). The blue and red starts in panel A represent the time points at which the AU analysis was performed. All the experiments carried out with the oligomeric samples were performed within two days after generating the samples. This time window in highlighted in green in panel A. The average fraction of monomeric protein in the oligomeric samples during this time window is ca. 10% (ca. 7 % at day 0 and ca. 13 % at day 2). Importantly, this analysis demonstrates the remarkably high kinetic stability of the oligomeric species characterized in this study.
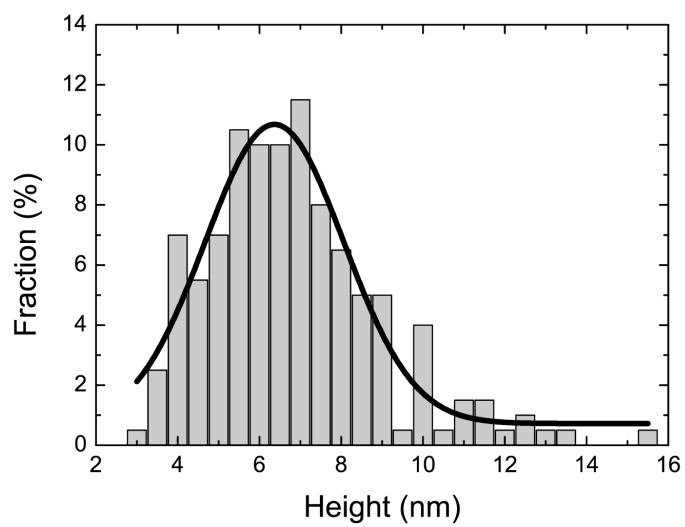
Figure S2. Height distribution of oligomeric species from AFM images. The arithmetic mean is 6.8 ± 2.1 nm, and the Gaussian mean is 6.4 ± 0.1 nm, n=200. For conditions, see Methods.
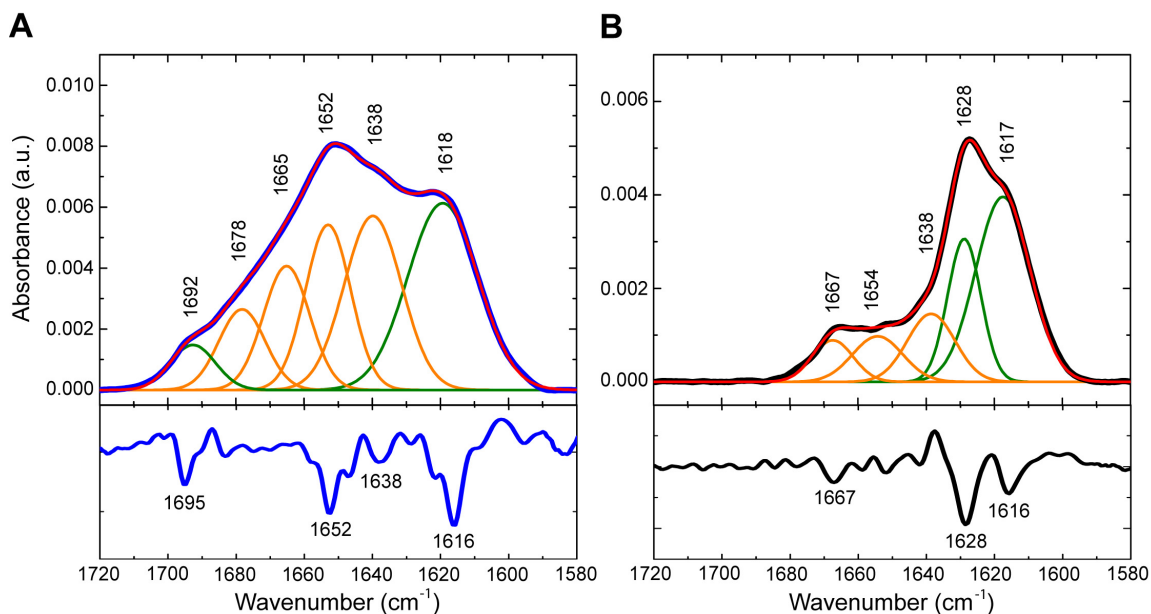
Figure S3. FT-IR analysis. Examples of the deconvolution analysis with Lorentzian curves and the second derivative analysis (bottom panel) of the FT-IR spectra of an oligomeric (A) and a fibrillar sample (B) are shown. For the spectra of the oligomeric samples (in blue), 6 Gaussian distributions were needed to fit the data, while only 5 were used for the spectra of the fibrillar samples (in black) (the fitting curves are shown in thin red line; the positions for each Gaussian distribution are also shown). There is a good agreement between the peaks of the Gaussian distributions obtained by the fitting of each spectrum and the negative peaks identified in the second derivative. The Gaussian distributions highlighted in green correspond to absorbance bands previously assigned to β-sheet secondary structure (Cerf E. *et al.*, 2009) and those highlighted in orange were attributed to the absorbance of random-coil regions as both oligomeric and fibrillar forms of the protein do not seem to possess α-helical content according to the far-UV CD analysis. This assignment was used to estimate the relative fraction of β-sheet content in each protein sample (note that the values obtained in this way represent only estimates).
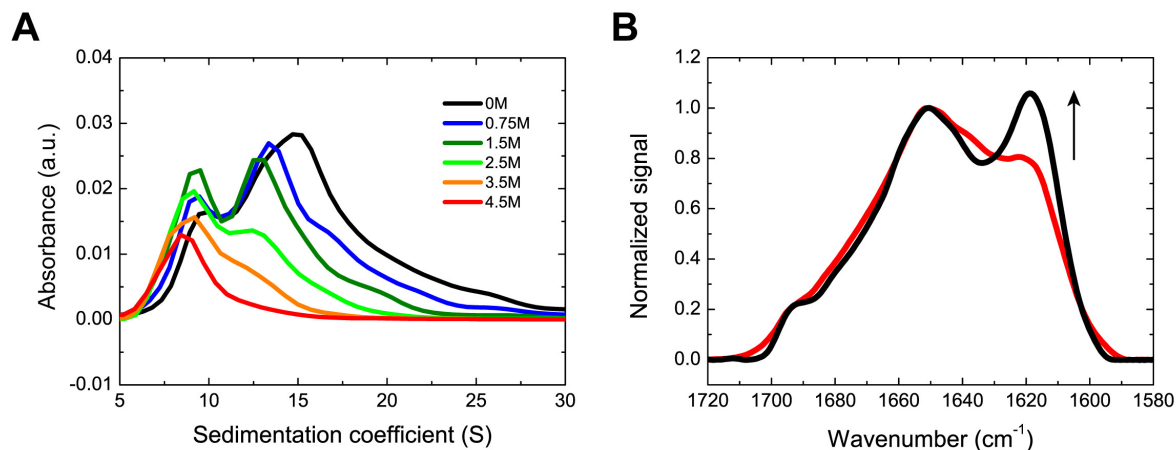
Figure S4. AU and FT-IR analysis of αS oligomeric samples generated by reusing the flow-through solution that passed through the 100 kDa cut-off filters. A) Sedimentation velocity analysis of an oligomeric sample generated from the flow-through solution of the 100 kDa filters during the protocol to isolate oligomeric species. The different sedimentation profiles correspond to the oligomeric species present in the sample after incubating the sample at different urea concentrations (as indicated) for 6 h. The effect of increasing urea concentrations on the size distribution of these oligomeric species generated from the flow-through solution is virtually identical to that found for oligomers generated from freshly purified monomers (see Figure 3 in the main text), although the former is slightly enriched in larger oligomeric species, suggesting that the flow-through solutions contain oligomeric species that can potentially act as seeds in subsequent cycles of lyophilization. B) Comparison between the FT-IR spectra of the oligomeric sample generated with freshly prepared monomeric protein (red line) and reused flow-through solutions (black line); the oligomeric samples generated with the flow-through solutions present a higher averaged β-sheet content (ca. 5% increase) than the oligomeric samples prepared with freshly purified momomeric protein, in agreement with the AU/CD combined analysis of oligomeric samples at different urea concentrations (see Figure 3 in the main text).
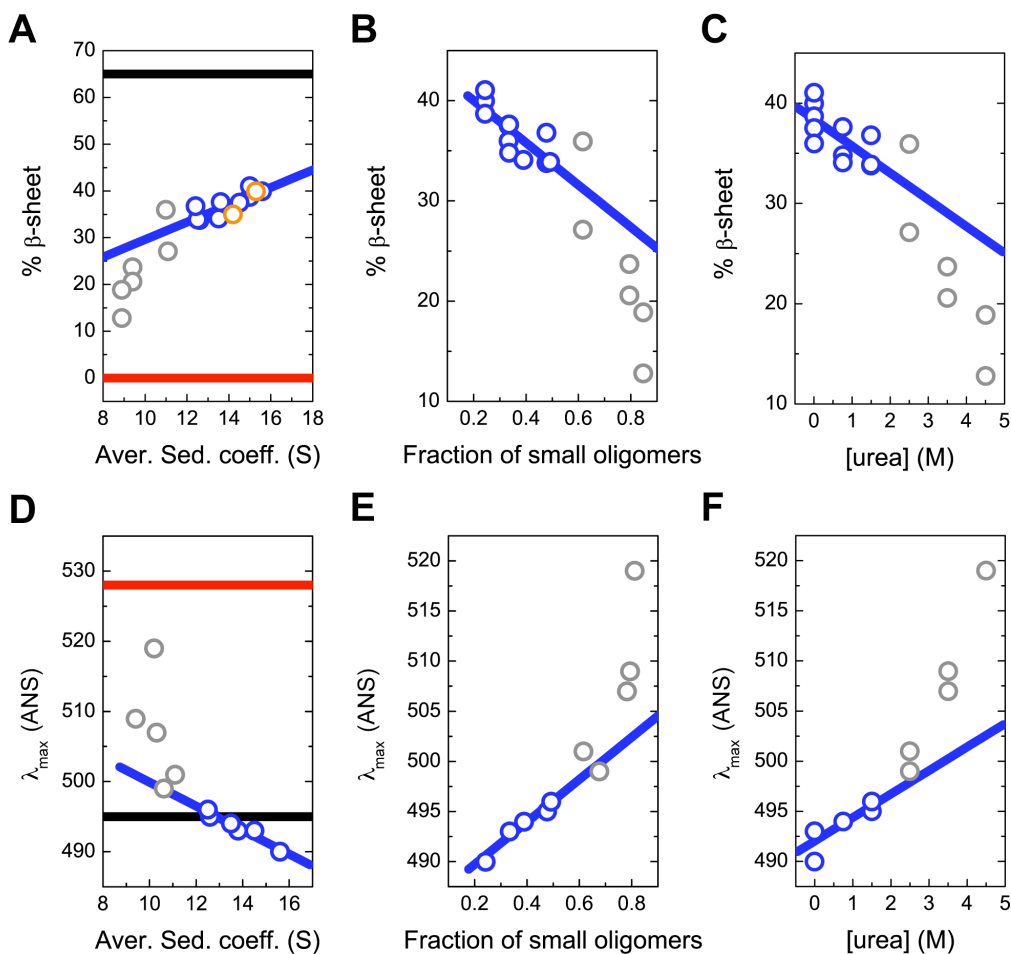
Figure S5. Detailed analysis of the structural properties of oligomers as a function of their size. The averaged secondary structure content (represented as % β-sheet) and the extent of hydrophobic surface exposed to the solvent (represented as wavelength of the maximum ANS fluorescence emission) of the oligomers present at different concentrations of urea were correlated with the averaged sedimentation coefficient obtained by AU with the same samples (A and D, respectively), the fraction of small oligomers estimated by AU (B and E, respectively) and the concentration of urea (C and F, respectively). Oligomeric samples prepared with freshly purified monomeric protein and oligomers generated from the flow-through solution collected from a previous oligomer purification process were both used for this analysis. Both structural parameters correlate linearly with the size parameters and the concentration of urea for the samples at 0-1.5 M urea concentrations (blue symbols), but they deviate significantly at higher urea concentrations (grey symbols), with larger deviations at the highest urea concentrations used, which indicates that at those conditions ([urea] > 1.5 M), the high concentration of urea present in the sample is affecting the folding of the oligomers in addition to disaggregating them. These data were therefore excluded from the analysis of the correlation between size and structure of the oligomers (blue lines in Figure 3c-d in the main text). The orange symbols in panel a) represent the data obtained by FT-IR for an oligomeric sample at 0 M urea prepared with freshly purified monomeric protein or with the flow-through collected from a previous oligomer purification process, clearly showing the dependency of the secondary structure content with the size of the oligomers.
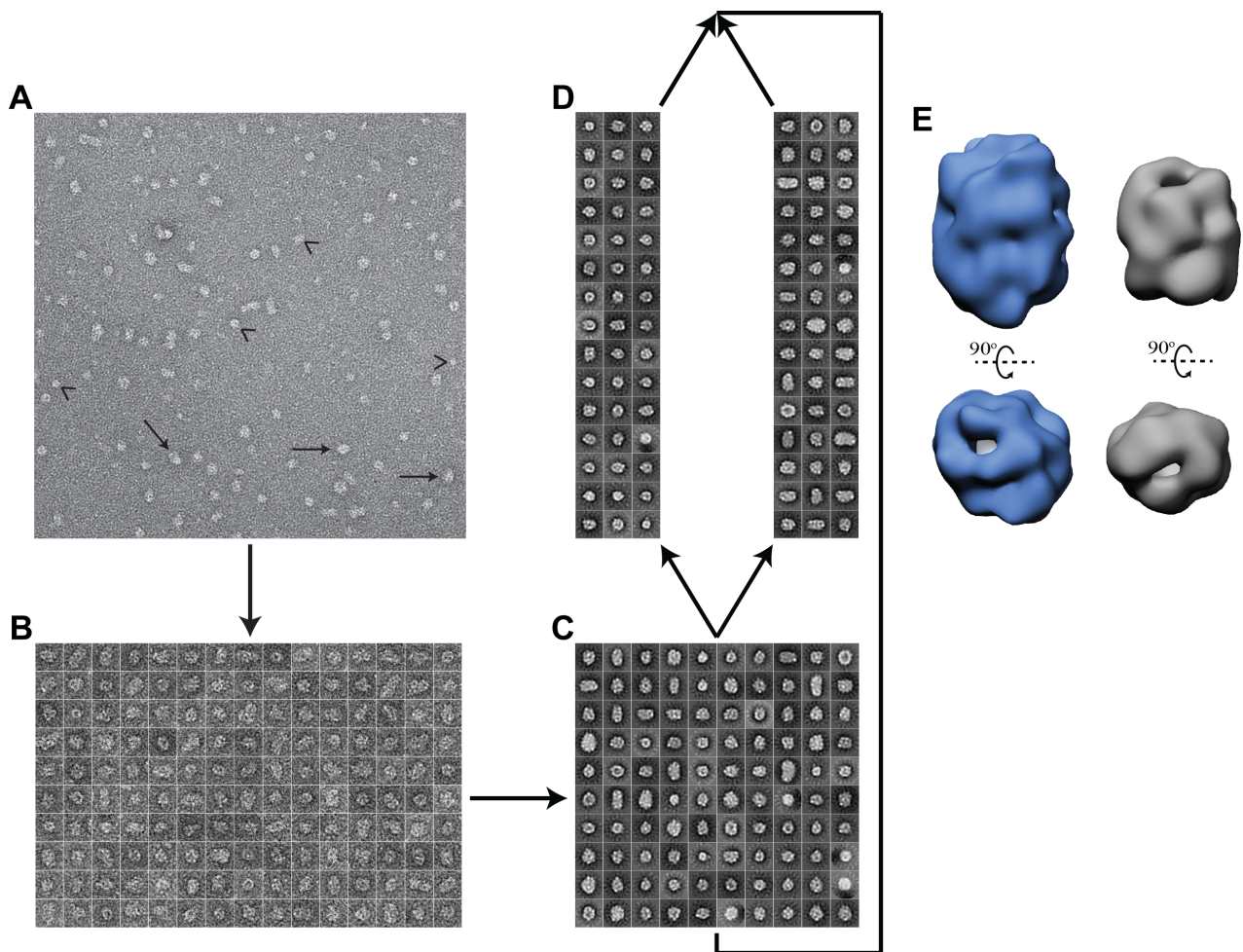
Figure S6. A scheme of the classification and 3D reconstruction procedure. A) An example of a negative staining micrograph of αS oligomers. Arrows point to large particles whereas arrowheads refer to small particles. B) Gallery of individual particles selected from the scanned micrographs (17242 and 7776 particles were manually selected from negatively stained and frozen samples respectively). C) "Clustering 2D" (CL2D), multi-reference free-pattern refinement approach was carried out with normalized particles. D) The generated class averages and assigned particles were separated according to their sizes as indicated by AU. Additional rounds of CL2D classification were applied to the separated particles, resulting in 60% of negatively stained particles and 46% of vitrified particles being assigned to the small size group. The large size group (15 S oligomeric subgroup) comprised of 40% and 54% of negatively stained and frozen particles respectively. E) Two orthogonal views of the 3D reconstructions corresponding to the large, 15S, (left) and small, 10S, (right) oligomeric subgroups.
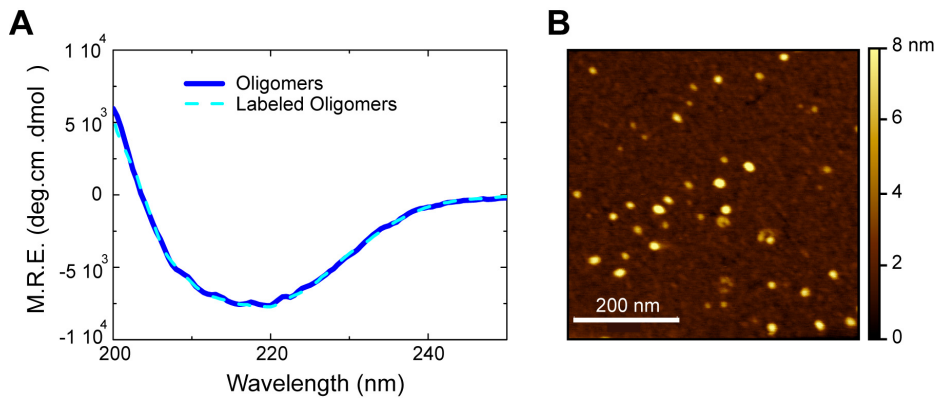
Figure S7. Morphological and structural comparison of unlabeled and fluorescently-labeled oligomers. a) The far-UV CD spectrum of the unlabeled (continuous dark blue line) and fluorescently-labeled oligomers (dotted light blue line) are identical. b) Representative of an AFM image of fluorescently-labeled oligomers. The morphology and overall dimensions for the unlabeled and labeled oligomers are very similar.
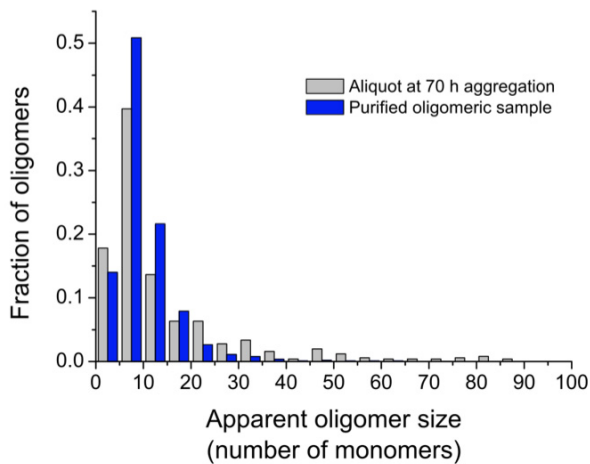
Figure S8. Estimation of the size distribution by smFRET experiments. Comparison of the size distributions obtained by smFRET experiments of a purified oligomeric sample (blue bars) and of oligomeric species present in an aliquot of an aggregating sample taken at ca. 70 h after the aggregation reaction was initiated, the time at which we observed a maximum accumulation of toxic oligomers during amyloid-fibril formation *in vitro* (Cremades N., *et al*., 2012) (grey bars). Both samples show relatively similar apparent size distributions according to smFRET analysis, with the majority of the oligomers presenting apparent sizes between 5-15mers. The apparent size distributions obtained by smFRET differ significantly from those obtained by AU at bulk conditions, which could be partially explained by possible disaggregation of oligomers upon dilution from bulk (μM) to sm (pM) conditions.
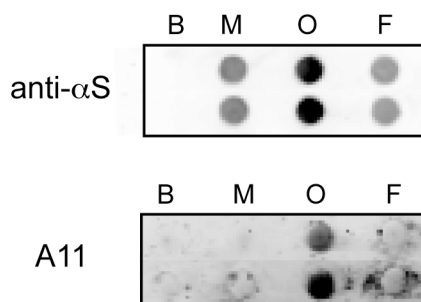
Figure S9. Dot-blot analysis of the different αS species. The blots were probed with anti-αS (Transduction Laboratories, Lexington, Kentucky, USA) and A11 (Millipore) antibodies. Duplicates for buffer solution as control (B), monomeric solution (M), oligomeric solution (O) and fibrillar solution (F) are shown for each antibody. Although A11 antibody was originally raised against an oligomeric species of Aβ peptide, it has also been reported to bind oligomeric forms, but not monomeric or fibrillar forms, of many other unrelated amyloidogenic peptides (Kayed, R., et al., 2003). Dot blot assays were performed by applying 5 μg of purified monomeric, oligomeric or fibrillar αS to a 0.2 μm nitrocellulose membrane (Millipore) mounted on a manifold. Samples were vacuum-filtered and washed twice with 100 μl of PBS. Purified αS fibrils were loaded after 5 cycles of sonication (10 s pulse, 50 s pause at 10 of amplitude) in order to facilitate their absorption to the membrane. Membranes were then blocked with 5% BSA in PBS for 1 h at room temperature and then probed overnight at 4°C with either anti-αS or A11 primary antibodies at 1:2000 and 1:500 of dilution in 5% BSA in PBS, respectively. Anti-αS and A11 probed membranes were then washed three times for 10 min with 0.01% Tween-20 in PBS, and subsequently incubated for 1 h at room temperature with Alexa Fluor-488 goat anti-mouse and Alexa Fluor-488 goat anti-rabbit secondary antibodies (Invitrogen) respectively at 1:5000 in 5% BSA, 0.01% Tween-20 in PBS. Finally, the excess of secondary antibody was removed by washing the membranes three times with 0.01% Tween-20 in PBS. Immunofluorescence quantification was done on a Typhoon Trio scanner (Amersham Bioscience) and the images were analyzed with the program ImageQuant TL v2005 software (Amersham Bioscience). It was particularly difficult to get similar amounts of each protein species adsorbed onto the membrane because of the large difference in size between the species (hence the use of sonicated fibrils). We tested different membranes with different pore sizes, and the best result in terms of an equilibrated protein adsorption onto the membrane for all the species was found with the 0.2 μm nitrocellulose membrane (Millipore). The assessment of the amount of protein adsorbed onto the membrane was performed using the polyclonal antibody anti-αS (Transduction Laboratories, Lexington, Kentucky, USA) that recognizes all the protein species (epitope: residues 15-123 from rat αS). The signal obtained for each protein species when using A11 was therefore compared with the relative amount of protein species adsorbed onto the membrane obtained using anti-αS antibody.
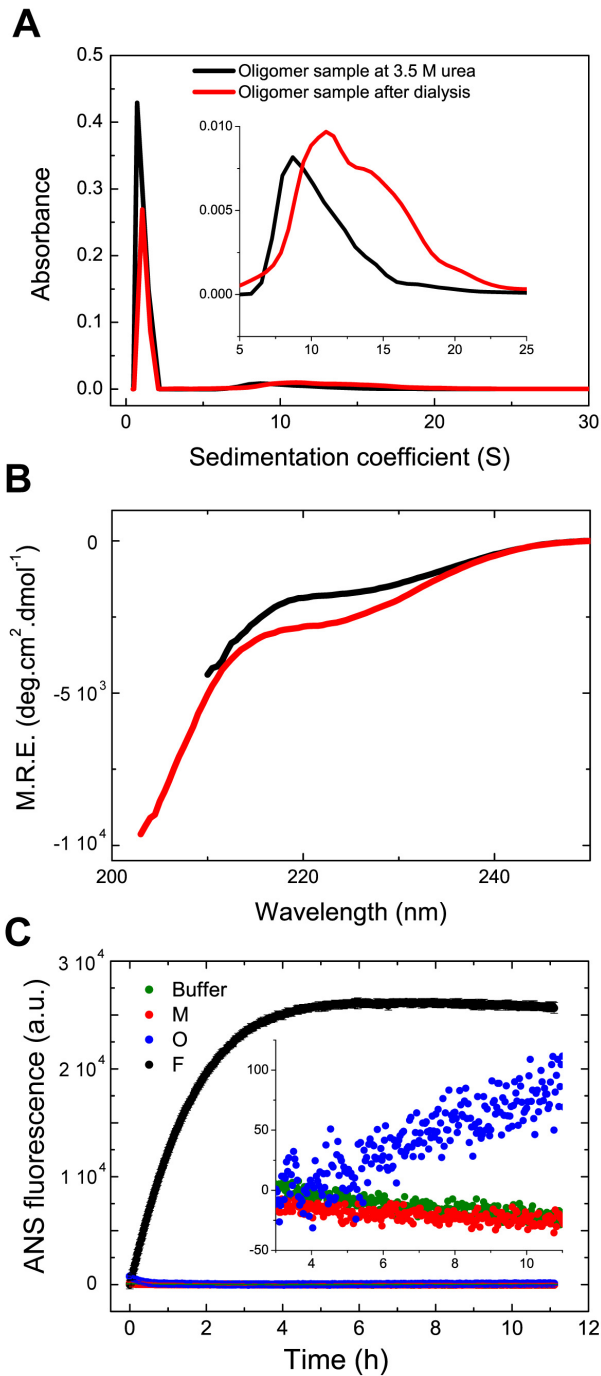
Figure S10. Comparison of the elongation capabilities of αS oligomeric and fibrillar structures. The purified 10S oligomers are able to elongate by monomer addition to generate larger oligomers. A) In the presence of 3.5M urea, the oligomeric distribution of a purified oligomeric sample is essentially composed only of the 10S subgroup of oligomers (black line). When the sample was dialyzed against PBS buffer pH 7.4 to remove the urea, an increase in the mass fraction of oligomers and the appearance of larger oligomers were observed, along with a concomitant reduction of the amount of monomeric protein in the sample (red line). B) A similar conclusion is obtained when the samples were analyzed by far-UV CD. C) Kinetics of elongation of the oligomeric (blue symbols) and the fibrillar (black symbols) structure followed by ANS fluorescence. Protein samples contained 20 μM of either oligomeric or fibrillar species, 100 μM of

monomeric protein and 250 µM of ANS in PBS buffer pH 7.4. Controls without protein (green symbols) and with only monomeric protein in the sample (red symbols) were also run. Samples were incubated in clear-bottomed half-area 96-well plates (Corning, NY) in a Clariostar plate reader (BMG Labtech, Aylesbury, UK) at 37°C without shaking and the kinetics of elongation was monitored by bottom reading of fluorescence intensity using 362 ± 25 nm excitation and 485 ± 20 nm emission. The data correspond to the average and standard deviation of triplicates measured in the same plate. In order to reduce the effects of clumping in the fibrillar sample which may influence the kinetics of elongation, fibrils prepared as described previously (see Supplemetal Experimental Procedures) were sonicated for 1 min using a probe sonicator (Bandelin, Sonopuls HD 2070) using 10% maximum power and 30% cycles. 10 µM of these sonicated fibrils were further incubated with 100 µM of monomer in 500 µl PBS for 13-15h under quiescent conditions (no shaking). Each sample was then centrifuged (15 min at 13200 rpm) and the resulting pellet washed twice with PBS before being resuspended into the appropriate volume of PBS. These resulting fibrils were sonicated for 20 seconds, 30% cycles, 10% maximum power in order to get fibrillar species with similar sizes to that of the oligomers (arithmetic mean of 5.0 ± 2.7 nm in height and 50 ± 50 nm in length).

Supplemental References

1. Roodveldt C, *et al.* (2012) A rationally designed six-residue swap generates comparability in the aggregation behavior of alpha-synuclein and beta-synuclein. *Biochemistry* 51(44):8771-8778.
2. Lorenzen N, *et al.* (2014) The role of stable alpha-synuclein oligomers in the molecular events underlying amyloid formation. *J Am Chem Soc* 136(10):3859-3868.
3. Volles MJ, *et al.* (2001) Vesicle permeabilization by protofibrillar alpha-synuclein: implications for the pathogenesis and treatment of Parkinson's disease. *Biochemistry* 40(26):7812-7819.
4. van Rooijen BD, Claessens MM, & Subramaniam V (2009) Lipid bilayer disruption by oligomeric alpha-synuclein depends on bilayer charge and accessibility of the hydrophobic core. *Biochim Biophys Acta* 1788(6):1271-1278.
5. Giehm L, Svergun DI, Otzen DE, & Vestergaard B (2011) Low-resolution structure of a vesicle disrupting α-synuclein oligomer that accumulates during fibrillation. *Proc Natl Acad Sci U S A* 108(8):3246-3251.
6. Lorenzen N, Lemminger L, Pedersen JN, Nielsen SB, & Otzen DE (2014) The N-terminus of alpha-synuclein is essential for both monomeric and oligomeric interactions with membranes. *FEBS Lett* 588(3):497-502.
7. Celej MS, *et al.* (2012) Toxic prefibrillar alpha-synuclein amyloid oligomers adopt a distinctive antiparallel beta-sheet structure. *Biochem J* 443(3):719-726.
8. Zhang H, Griggs A, Rochet JC, & Stanciu LA (2013) In vitro study of alpha-synuclein protofibrils by cryo-EM suggests a Cu(2+)-dependent aggregation pathway. *Biophys J* 104(12):2706-2713.
9. Gallea JI & Celej MS (2014) Structural Insights into Amyloid Oligomers of the Parkinson Disease-related Protein alpha-Synuclein. *J Biol Chem* 289(39):26733-26742.
10. Danzer KM, *et al.* (2007) Different species of alpha-synuclein oligomers induce calcium influx and seeding. *J Neurosci* 27(34):9220-9232.

11. Campioni S*, et al.* (2014) The presence of an air-water interface affects formation and elongation of alpha-Synuclein fibrils. *J Am Chem Soc* 136(7):2866-2875.
12. Cremades N*, et al.* (2012) Direct observation of the interconversion of normal and toxic forms of alpha-synuclein. *Cell* 149(5):1048-1059.
13. Hoyer W*, et al.* (2002) Dependence of alpha-synuclein aggregate morphology on solution conditions. *J Mol Biol* 322(2):383-393.
14. Muller R*, et al.* (2010) Molecular weight determination of high molecular mass (glyco)proteins using CGE-on-a-chip, planar SDS-PAGE and MALDI-TOF-MS. *Electrophoresis* 31(23-24):3850-3862.
15. Cerf E*, et al.* (2009) Antiparallel beta-sheet: a signature structure of the oligomeric amyloid beta-peptide. *Biochem J* 421(3):415-423.
16. Miyazawa T & Blout ER (1961) The infared spectra of polypeptides in various conformations: amide I and amide II bands. *J. Am. Chem. Soc.* 83(3):712-719.
17. Cardamone M & Puri NK (1992) Spectrofluorimetric assessment of the surface hydrophobicity of proteins. *Biochem J* 282 (Pt 2):589-593.
18. Mindell JA & Grigorieff N (2003) Accurate determination of local defocus and specimen tilt in electron microscopy. *J Struct Biol* 142(3):334-347.
19. Marabini R*, et al.* (1996) Xmipp: An Image Processing Package for Electron Microscopy. *J Struct Biol* 116(1):237-240.
20. Scheres SH (2010) Classification of structural heterogeneity by maximum-likelihood methods. *Methods Enzymol* 482:295-320.
21. Sorzano CO*, et al.* (2010) A clustering approach to multireference alignment of single-particle projections in electron microscopy. *J Struct Biol* 171(2):197-206.
22. Ludtke SJ, Baldwin PR, & Chiu W (1999) EMAN: semiautomated software for high-resolution single-particle reconstructions. *J Struct Biol* 128(1):82-97.
23. Crowther RA, Amos LA, Finch JT, De Rosier DJ, & Klug A (1970) Three dimensional reconstructions of spherical viruses by fourier synthesis from electron micrographs. *Nature* 226(5244):421-425.
24. Pettersen EF*, et al.* (2004) UCSF Chimera--a visualization system for exploratory research and analysis. *J Comput Chem* 25(13):1605-1612.
25. Orte A, Clarke R, Balasubramanian S, & Klenerman D (2006) Determination of the fraction and stoichiometry of femtomolar levels of biomolecular complexes in an excess of monomer using single-molecule, two-color coincidence detection. *Anal Chem* 78(22):7707-7715.
26. Weinstein JN, Yoshikami S, Henkart P, Blumenthal R, & Hagins WA (1977) Liposome-cell interaction: transfer and intracellular release of a trapped fluorescent marker. *Science* 195(4277):489-492.